Chinese Journal of Aeronautics, (2020), xxx(xx): xxx–xxx

Chinese Society of Aeronautics and Astronautics
& Beihang University

Chinese Journal of Aeronautics

cja@buaa.edu.cn
www.sciencedirect.com

Loopy belief propagation based data association for extended target tracking

Zhenzhen SU, Hongbing JI *, Yongquan ZHANG

School of Electronic Engineering, Xidian University, Xi'an 710071, China

Received 5 September 2019; revised 13 October 2019; accepted 24 December 2019

KEYWORDS

Belief propagation;
Data association;
Extended target;
Graphical model;
Simplified measurement set;
Target tracking

Abstract The data association problem of multiple extended target tracking is very challenging because each target may generate multiple measurements. Recently, the belief propagation based multiple target tracking algorithms with high efficiency have been a research focus. Different from the belief propagation based Extended Target tracking based on Belief Propagation (ET-BP) algorithm proposed in our previous work, a new graphical model formulation of data association for multiple extended target tracking is proposed in this paper. The proposed formulation can be solved by the Loopy Belief Propagation (LBP) algorithm. Furthermore, the simplified measurement set in the ET-BP algorithm is modified to improve tracking accuracy. Finally, experiment results show that the proposed algorithm has better performance than the ET-BP and joint probabilistic data association based on the simplified measurement set algorithms in terms of accuracy and efficiency. Additionally, the convergence of the proposed algorithm is verified in the simulations.

1. Introduction

Multiple Target Tracking (MTT) is aimed at estimating the number and states of multiple targets based on the measurements of sensors. MTT problems can be divided into two main categories: Multiple Point Target Tracking (MPTT)[1,2] and Multiple Extended Target Tracking (METT).[3–6] In MPTT, each point target generates at most one measurement per time step. Different from MPTT, METT deals with extended targets whose echo occupies one or more than one resolution cell and generates one or more than one measurement per time step. Recently, due to the significant improvement in sensors resolution, METT is brought to the forefront and widely used in many applications such as autonomous driving, surveillance, sensor networks, mobile robotics, and so on. Besides, the measurement-to-track association problem is a crucial issue in MTT applications.

The existing MTT algorithms include vector model based algorithms[7] and set model based algorithms,[8] in which the multiple target states and measurements are modeled as random vectors and Random Finite Sets (RFSs), respectively. These algorithms generally have high complexity and cannot scale well with system parameters. Because of such drawbacks, they are not suitable for the applications with a large number

* Corresponding author.
E-mail address: hbji@xidian.edu.cn (H. JI).
Peer review under responsibility of Editorial Committee of CJA.

ELSEVIER Production and hosting by Elsevier

https://doi.org/10.1016/j.cja.2020.01.004
1000-9361 © 2020 Chinese Society of Aeronautics and Astronautics. Production and hosting by Elsevier Ltd.

Please cite this article in press as: SU Z et al. Loopy belief propagation based data association for extended target tracking, *Chin J Aeronaut* (2020), https://doi.org/10.1016/j.cja.2020.01.004

of measurements and targets. However, it is worth noting that the graphical model[9–11] is an essential tool for inference and learning because the Belief Propagation (BP) algorithm can provide a principled approximation of the optimum Bayesian inference.[12] The BP algorithm has been successfully applied to many fields, such as sensor networks,[13] cooperative localization,[14] communication receivers,[15] and channel codes.[16] At the same time, BP based MTT algorithms have gradually become a research focus.

The RFS based algorithms generally calculate the approximation of the joint posterior Probability Density Function (PDF). Different from these algorithms, the BP algorithm can approximate the marginal posterior PDFs for each target. Recently, the BP algorithm is particularly attractive for MTT,[2,12,17–21] because it enables an efficient calculation of the marginal posterior PDFs for the data association problem. Some MPTT algorithms based on graphical models have been proposed. The Loopy BP (LBP) algorithm was used to solve the data association problem in situations where each sensor has a narrow field of view.[17] It was also used to solve the data association problem in situations where there are a fixed number of targets observed by a single sensor.[18] Furthermore, the algorithm was extended to solve the multisensor-multitarget detection-estimation problem,[19] which allows for an unknown and time-varying number of targets. The BP based algorithms above are vector modeled, where the joint posterior PDF is expressed in random vectors. The LBP algorithm was used to approximate the posterior PDF expressed by RFSs,[2] resulting in the Track-Oriented Marginal MeMBer/Poisson (TOMB/P) filter and the Measurement-Oriented Marginal MeMBer/Poisson (MOMB/P) filter. The approximation by the LBP algorithm dramatically improves the efficiency of the Poisson Multi-Bernoulli Mixture (PMBM) filter and promotes its application.

Although graphical models perform well in MPTT, they do not perform so well in METT due to some challenges. Because an extended target can generate one or multiple measurements per time step, the BP based algorithms in MPTT are no longer applicable in METT, and the data association problem in METT is more complicated than that in MPTT. Thus, it is important to solve the data association problem efficiently in METT. The BP based METT (ET-BP) algorithm has been proposed in our previous work,[20] in which the BP algorithm is applied to METT based on a Simplified Measurement Set (SMS). However, the extension state estimation has a significant deviation. In this paper, the LBP based METT algorithm is proposed, named ET-LBP, which overcomes the deviation of the extension state estimation in the ET-BP algorithm. Firstly, we formulate the data association problem in METT based on a new graphical model. Then, the graphical model is solved by the LBP algorithm to obtain the marginal PDFs of the joint posterior PDFs. In order to implement the ET-LBP algorithm with high efficiency and accuracy, an improved scheme to the SMS is proposed. Finally, the simulation results show that the ET-LBP algorithm is superior to the ET-BP and Joint Probabilistic Data Association based on the SMS (JPDA-SMS) algorithms.[20] The Improved SMS (ISMS) has better performance than the SMS in tracking.

The rest of this paper is organized as follows. In Section 2, the basic assumptions, the factor graphs and the LBP algorithm are reviewed. Then, the data association problem in METT, the ET-LBP algorithm and the ISMS are proposed in Section 3. Section 4 illustrates the simulation results, and conclusions are given in Section 5.

2. Backgrounds

In this section, the underlying assumptions of METT are reviewed in Section 2.1, and the factor graphs and the LBP algorithm are introduced in Section 2.2.

2.1. Basic assumptions

The underlying assumptions in the METT algorithms are given in this subsection. At time step k, let $\boldsymbol{\xi}_k = \{\boldsymbol{\xi}_k^i\}_{i=1}^{n_k}$ denote the extended target states of n_k targets. There are some assumptions about the extended target state as follows.[22,23]

(1) The number of measurements generated by the extended target $\boldsymbol{\xi}_k$ is Poisson distributed, with a Gamma distributed rate γ_k. Furthermore, the measurement rate is conditionally independent of the target's kinematics and extension.
(2) The target's kinematics and extension can be decomposed into a random vector $\boldsymbol{x}_k$ and a random matrix $\boldsymbol{X}_k$.

Thus, the ith extended target state can be modeled as $\boldsymbol{\xi}_k^i = \{\gamma_k^i, \boldsymbol{x}_k^i, \boldsymbol{X}_k^i\}$, including a measurement rate γ_k^i, a kinematic state vector $\boldsymbol{x}_k^i$ and an extension state matrix $\boldsymbol{X}_k^i$. The vector $\boldsymbol{x}_k^i$ includes the target's kinematics, and the matrix $\boldsymbol{X}_k^i$ consists of the target's size and shape. At time step k, the sensor produces m_k measurements $\boldsymbol{Z}_k = \{\boldsymbol{z}_k^i\}_{i=1}^{m_k}$, and the cumulative measurement is represented by $\boldsymbol{Z}^k = \{\boldsymbol{Z}_l\}_{l=1}^{k}$. The conditional probability of $\boldsymbol{\xi}_k^i$ given $\boldsymbol{Z}^k$ is defined as Gamma Gaussian Inverse Wishart (GGIW) distribution

$$\begin{aligned} f(\boldsymbol{\xi}_k^i|\boldsymbol{Z}^k) &= f(\gamma_k^i|\boldsymbol{Z}^k) f(\boldsymbol{x}_k^i|\boldsymbol{X}_k^i, \boldsymbol{Z}^k) f(\boldsymbol{X}_k^i|\boldsymbol{Z}^k) \\ &= \mathrm{GAM}\left(\gamma_k^i; \alpha_{k|k}^i, \beta_{k|k}^i\right) \mathcal{N}\left(\boldsymbol{x}_k^i; \boldsymbol{x}_{k|k}^i, \boldsymbol{P}_{k|k}^i \otimes \boldsymbol{X}_k^i\right) \\ &\quad \times \mathrm{IW}\left(\boldsymbol{X}_k^i; \vartheta_{k|k}^i, \boldsymbol{V}_{k|k}^i\right) \end{aligned} \tag{1}$$

where $\mathrm{GAM}(\gamma; \alpha, \beta)$ denotes a Gamma PDF defined over the variable γ with shape parameter α and inverse scale parameter β, $\mathcal{N}(\boldsymbol{x}; \boldsymbol{m}, \boldsymbol{P})$ denotes a multivariate Gaussian distribution defined over the variable vector $\boldsymbol{x}$ with mean vector $\boldsymbol{m}$ and covariance matrix $\boldsymbol{P}$, and $\mathrm{IW}(\boldsymbol{X}; \vartheta, \boldsymbol{V})$ denotes an inverse Wishart PDF defined over the matrix $\boldsymbol{X}$ with degrees of freedom ϑ and parameter matrix $\boldsymbol{V}$. $\otimes$ represents Kronecker product. Thus, the set of GGIW parameters is $\left\{\alpha_{k|k}^i, \beta_{k|k}^i, \boldsymbol{x}_{k|k}^i, \boldsymbol{P}_{k|k}^i, \vartheta_{k|k}^i, \boldsymbol{V}_{k|k}^i\right\}$. The measurement rate, the kinematic state and the extension state can be estimated by

$$\hat{\gamma}_{k|k}^i = \frac{\alpha_{k|k}^i}{\beta_{k|k}^i} \tag{2}$$

$$\hat{\boldsymbol{x}}_{k|k}^i = \boldsymbol{x}_{k|k}^i \tag{3}$$

and

$$\hat{\boldsymbol{X}}_{k|k}^i = \frac{\boldsymbol{V}_{k|k}^i}{\vartheta_{k|k}^i - 2d - 2} \tag{4}$$

Please cite this article in press as: SU Z et al. Loopy belief propagation based data association for extended target tracking, *Chin J Aeronaut* (2020), https://doi.org/10.1016/j.cja.2020.01.004

respectively, where d is the dimension of $\boldsymbol{X}_k^i$.

The random matrix model limits the extended targets to be shaped as ellipses, but the model is applicable to many real scenarios.[24] Owing to the specific form of the conditional Gaussian distribution, where the covariance is the Kronecker product of the matrix $\boldsymbol{P}_{k|k}^i$ and the extent matrix, the kinematic vector cannot include non-linear dynamics, such as the turn rate. The extended target can also be modeled by factorized state density. Although the factorized state density has theoretical drawback, the kinematic vector can include non-linear dynamics[25]. In addition to Assumptions (1) and (2), there are some other assumptions[24] as follows.

(1) The multiple extended target states evolve independently based on the transition densities $f(\boldsymbol{x}_k|\boldsymbol{x}_{k-1},\boldsymbol{X}_k)$ and $f(\boldsymbol{X}_k|\boldsymbol{X}_{k-1})$.[26]
(2) The probability that target i generates a measurement cell at time step k is $p_{\mathrm{D}}(\boldsymbol{\xi}_k^i)$. Consequently, the probability that no measurement originates from target i is $1-p_{\mathrm{D}}(\boldsymbol{\xi}_k^i)$.
(3) Each extended target can generate one or more than one measurement per time step. Each measurement is from one and only one extended target or clutter (false alarm).
(4) The number of clutter measurements at time step k obeys a Poisson distribution with mean μ_{c}.
(5) If target i does generate a measurement cell $\boldsymbol{Z}_k^i$ at time step k, the likelihood function[23] is

$$\begin{aligned} f(\boldsymbol{Z}_k^i|\boldsymbol{\xi}_k^i) &= f(\boldsymbol{Z}_k^i, m_k^i|\boldsymbol{\xi}_k^i) \\ &= f(m_k^i|\gamma_k^i)\prod_{\boldsymbol{z}\in\boldsymbol{Z}_k^i}\phi(\boldsymbol{z};\boldsymbol{x}_k^i,\boldsymbol{X}_k^i) \end{aligned} \tag{5}$$

where m_k^i is the number of measurements in $\boldsymbol{Z}_k^i$, and $\phi(\boldsymbol{z};\boldsymbol{x}_k^i,\boldsymbol{X}_k^i)$ is the spatial measurement distribution of target i.

(6) Measurements of each target are conditionally independent.

Under the assumptions above, the Bayesian framework[22] in tracking a single extended target is reviewed in Table 1, including prediction and updating.

In the prediction, $1/\eta_{k-1}$ is a forgetting factor using exponential forgetting. $\boldsymbol{I}_d$ is an identity matrix of dimension d. τ is a temporal decay constant. The evolution matrix $\boldsymbol{F}_{k|k-1}$ and the covariance $\boldsymbol{D}_{k|k-1}$ of Gaussian process noise are computed by

$$\boldsymbol{F}_{k|k-1} = \begin{bmatrix} 1 & T_{\mathrm{s}} & 0.5T_{\mathrm{s}}^2 \\ 0 & 1 & T_{\mathrm{s}} \\ 0 & 0 & \mathrm{e}^{-T_{\mathrm{s}}/\theta} \end{bmatrix} \tag{6}$$

$$\boldsymbol{D}_{k|k-1} = \sum\nolimits^2\left(1-\mathrm{e}^{-2T_{\mathrm{s}}/\theta}\right)\mathrm{diag}([0\quad 0\quad 1]) \tag{7}$$

respectively, where Σ is the scalar acceleration standard deviation, θ is the maneuver correlation time and T_{s} is the sampling time.

In the updating, $\bar{\boldsymbol{z}}_k^i$, $\boldsymbol{K}_{k|k-1}^i$, $\boldsymbol{S}_{k|k-1}^i$, $\boldsymbol{N}_{k|k-1}^i$ and $\bar{\boldsymbol{Z}}_{k|k-1}^i$ are the centroid measurement, gain matrix, innovation factor, innovation matrix and scatter matrix, respectively. $\boldsymbol{Z}_k^i$ represents the measurements associated with target i.

Table 1 Bayesian framework.

Prediction:	$\alpha_{k|k-1}^i = \alpha_{k-1|k-1}^i/\eta_{k-1}$
	$\beta_{k|k-1}^i = \beta_{k-1|k-1}^i/\eta_{k-1}$
	$\boldsymbol{x}_{k|k-1}^i = (\boldsymbol{F}_{k|k-1}\otimes\boldsymbol{I}_d)\boldsymbol{x}_{k-1|k-1}^i$
	$\boldsymbol{P}_{k|k-1}^i = \boldsymbol{F}_{k|k-1}\boldsymbol{P}_{k-1|k-1}^i\boldsymbol{F}_{k|k-1}^{\mathrm{T}} + \boldsymbol{D}_{k|k-1}$
	$\vartheta_{k|k-1}^i = \exp(-T_{\mathrm{s}}/\tau)\vartheta_{k-1|k-1}^i$
	$\boldsymbol{V}_{k|k-1}^i = \frac{\vartheta_{k|k-1}^i-d-1}{\vartheta_{k-1|k-1}^i-d-1}\boldsymbol{V}_{k-1|k-1}^i$
Updating:	$\alpha_{k|k}^i = \alpha_{k|k-1}^i + m_k^i$
	$\beta_{k|k}^i = \beta_{k|k-1}^i + 1$
	$\boldsymbol{x}_{k|k}^i = \boldsymbol{x}_{k|k-1}^i + \left(\boldsymbol{K}_{k|k-1}^i\otimes\boldsymbol{I}_d\right)\left(\bar{\boldsymbol{z}}_k^i - \boldsymbol{H}\boldsymbol{x}_{k|k-1}^i\right)$
	$\boldsymbol{P}_{k|k}^i = \boldsymbol{P}_{k|k-1}^i - \boldsymbol{K}_{k|k-1}^i\boldsymbol{S}_{k|k-1}^i\left(\boldsymbol{K}_{k|k-1}^i\right)^{\mathrm{T}}$
	$\vartheta_{k|k}^i = \vartheta_{k|k-1}^i + m_k^i$
	$\boldsymbol{V}_{k|k}^i = \boldsymbol{V}_{k|k-1}^i + \boldsymbol{N}_{k|k-1}^i + \bar{\boldsymbol{Z}}_{k|k-1}^i$
where	$\bar{\boldsymbol{z}}_k^i = \frac{1}{m_k^i}\sum_{\boldsymbol{z}_j\in\boldsymbol{Z}_k^i}\boldsymbol{z}_j$
	$\boldsymbol{K}_{k|k-1}^i = \boldsymbol{P}_{k|k-1}^i\boldsymbol{H}_k^{\mathrm{T}}\left(\boldsymbol{S}_{k|k-1}^i\right)^{\mathrm{T}}$
	$\boldsymbol{S}_{k|k-1}^i = \boldsymbol{H}_k\boldsymbol{P}_{k|k-1}^i\boldsymbol{H}_k^{\mathrm{T}} + \frac{1}{m_k^i}$
	$\boldsymbol{N}_{k|k-1}^i = \left(\boldsymbol{S}_{k|k-1}^i\right)^{-1}\left(\bar{\boldsymbol{z}}_k^i - \boldsymbol{H}\boldsymbol{x}_{k|k-1}^i\right)\left(\bar{\boldsymbol{z}}_k^i - \boldsymbol{H}\boldsymbol{x}_{k|k-1}^i\right)^{\mathrm{T}}$
	$\bar{\boldsymbol{Z}}_{k|k-1}^i = \sum_{\boldsymbol{z}_j\in\boldsymbol{Z}_k^i}(\boldsymbol{z}_j-\bar{\boldsymbol{z}}_k^i)(\boldsymbol{z}_j-\bar{\boldsymbol{z}}_k^i)^{\mathrm{T}}$

2.2. Factor graphs and LBP

The factor graph[27] is a graphical model, consisting of variable nodes and factor nodes, in which the variable nodes represent random variables and the factor nodes describe the dependencies between the random variables. The graphical models also include undirected graphical models (Markov random fields)[28] and directed graphical models (Bayesian networks).[29] In a factor graph, if some variables are dependent on each other in a factor node, then the variable nodes and the factor node are adjacent, connected by edges. For example, suppose that a factor graph includes variable nodes $n\in N$ and factor nodes $f\in F$ with neighbor nodes v_f, where N and F represent all the variable nodes and factor nodes in the factor graph, respectively. The joint PDF $f(\boldsymbol{x})$ can be factorized as

$$f(\boldsymbol{x}) \propto \prod_n \psi(x_n)\prod_f \varphi(x_{v_f}) \tag{8}$$

where $\psi(\cdot)$ and $\varphi(\cdot)$ are the PDFs of variables and factors, respectively.

Then, the BP algorithm is able to marginalize the joint PDF $f(\boldsymbol{x})$ by calculating the marginal PDFs $f(x_n)$ with a small computational cost. The BP is a message passing algorithm, which calculates messages of each variable node, and messages passing between variable nodes and factor nodes. The message sent from variable node x_n to factor node f is given by

$$u_{n\to f}(x_n) = \psi(x_n)\prod_{\zeta\in v_n\backslash f} u_{\zeta\to n}(x_n) \tag{9}$$

where v_n denotes the factor nodes involving the variable node x_n and $v_n \backslash f$ is the set of elements in v_n except f. $u_{f\to n}(x_n)$ is the message sent from factor node f to variable node x_n, given by

$$u_{f\to n}(x_n) = \int \varphi(x_{v_f}) \prod_{\zeta \in v_f \backslash n} u_{\zeta\to n}(x_\zeta) \mathrm{d}x_{v_f \backslash n} \tag{10}$$

Finally, the message of variable node x_n is calculated by

$$f(x_n) = \psi(x_n) \prod_{\zeta \in v_n} u_{\zeta\to n}(x_n) \tag{11}$$

Furthermore, the marginal PDF of variable x_n can also be obtained by

$$\hat{f}(x_n) = f(x_n) / \int f(x'_n) \mathrm{d}x'_n \tag{12}$$

It is worth noting that the BP algorithm becomes the LBP algorithm if it is applied to a factor graph with loops. The LBP algorithm performs iteratively, in which the entire message update process is repeated several times. Additionally, the LBP algorithm can be interpreted as a variational algorithm that aims to solve a constrained optimization problem.[30] Although the optimization problem is not convex, the marginal PDF obtained by the LBP algorithm has been shown with reasonable accuracy in many applications.[31,32] The LBP algorithm can also approximate the marginal PDFs well when the optimization problem is locally convex, and the starting point can be obtained in the region. Thus, if the optimization problem is constructed as convex,[33] the global optimum can be obtained by the resulting iterative message passing algorithm. Although they can result in more accurate marginal PDFs than using the LBP algorithm directly, the computational complexity becomes higher.

3. Proposed algorithm

In this section, the data association problem in METT is formulated in Section 3.1. Then, the ET-LBP algorithm is proposed to solve the data association problem in Section 3.2. Furthermore, the difference between the ET-LBP and ET-BP algorithms is analyzed in Section 3.3. At the same time, a tractable implementation of the ET-LBP algorithm is presented by improving the SMS in Section 3.4.

3.1. Data association in METT

Due to the uncertainty of extended target states and measurements, there exists a data association problem in METT. For example, at time step k, it is unknown whether an extended target generates any measurement (missed detection), whether a measurement is originated from any extended target (clutter and false alarm) or which extended target a measurement is originated from. It is worth noting that an extended target may generate one or more than one measurement per time step. In order to formulate the data association problem at time step k, we need to define the target-oriented association variables $\boldsymbol{A}_k = \{\boldsymbol{a}_k^i\}_{i=1}^{n_k}$ where $\boldsymbol{a}_k^i = [a_k^{i,1}, a_k^{i,2}, \cdots, a_k^{i,m_k}]$ with entries

$$a_k^{i,j} = \begin{cases} 1 & \text{if measurement } j \text{ is orignated from extended target } i \\ 0 & \text{if measurement } j \text{ is not orignated from extended target } i \end{cases} \tag{13}$$

Then, $\boldsymbol{a}_k^i \in \mathcal{A}$, where $\mathcal{A}$ is the set of all possible combinations of $\boldsymbol{a}_k^i$. At the same time, the measurement-oriented association variables $\boldsymbol{B}_k = [b_k^1, b_k^2, \cdots, b_k^{m_k}]$ where

$$b_k^j = \begin{cases} i & \text{if measurement } j \text{ is originated from extended target } i \\ 0 & \text{if measurement } j \text{ is clutter or false alarm} \end{cases} \tag{14}$$

In fact, $\boldsymbol{B}_k$ contains the same information as $\boldsymbol{A}_k$, which means that they are equivalent.

In METT, the goal of Bayesian estimation is to get the posterior PDF $f(\boldsymbol{\xi}_k|\boldsymbol{Z}^k)$. Based on the target-oriented association variables $\boldsymbol{a}_k^i = [a_k^{i,1}, a_k^{i,2}, \cdots, a_k^{i,m_k}]$ and Bayesian rule, the posterior PDF is given by

$$\begin{aligned} f(\boldsymbol{\xi}_k|\boldsymbol{Z}^k) &= \sum_{\boldsymbol{A}_k} f(\boldsymbol{\xi}_k, \boldsymbol{A}_k|\boldsymbol{Z}^k) \\ &\propto \sum_{\boldsymbol{A}_k} f(\boldsymbol{\xi}_k|\boldsymbol{Z}^{k-1}) f(\boldsymbol{Z}_k, \boldsymbol{A}_k|\boldsymbol{\xi}_k, \boldsymbol{Z}^{k-1}) \\ &= \sum_{\boldsymbol{A}_k} f(\boldsymbol{\xi}_k|\boldsymbol{Z}^{k-1}) f(\boldsymbol{Z}_k, \boldsymbol{A}_k|\boldsymbol{\xi}_k) \end{aligned} \tag{15}$$

where $f(\boldsymbol{\xi}_k|\boldsymbol{Z}^{k-1})$ can be obtained during the prediction based on the Chapman-Kolmogorov equation. Thus, the critical problem of Bayesian estimation is calculating the likelihood function $f(\boldsymbol{Z}_k, \boldsymbol{A}_k|\boldsymbol{\xi}_k)$. In the following, $f(\boldsymbol{Z}_k|\boldsymbol{\xi}_k, \boldsymbol{A}_k)$ and $f(\boldsymbol{A}_k|\boldsymbol{\xi}_k)$ will be formulated to obtain $f(\boldsymbol{Z}_k, \boldsymbol{A}_k|\boldsymbol{\xi}_k)$. The PDF of $\boldsymbol{A}_k$ conditioned on $\boldsymbol{\xi}_k$ is defined as

$$f(\boldsymbol{A}_k|\boldsymbol{\xi}_k) = \varphi(\boldsymbol{A}_k) \prod_{i=1}^{n_k} \left[P_{\mathrm{D}}(\boldsymbol{\xi}_k^i)^{\theta_{\mathrm{D}}(\boldsymbol{a}_k^i)} \left(1 - P_{\mathrm{D}}(\boldsymbol{\xi}_k^i)\right)^{1-\theta_{\mathrm{D}}(\boldsymbol{a}_k^i)} \right] \tag{16}$$

where $\varphi(\boldsymbol{A}_k)$ is the indicator function, expressing the constraint of Assumption (3) in Section 2.1, i.e.,

$$\varphi(\boldsymbol{A}_k) = \begin{cases} 0 & \forall j, \exists i_1, i_2 \in \{1,2,\ldots,n_k\}, \text{ st } i_1 \neq i_2 \text{ and } a_k^{i_1,j} = a_k^{i_2,j} = 1 \\ 1 & \text{otherwise} \end{cases} \tag{17}$$

and $\theta_{\mathrm{D}}(\boldsymbol{a}_k^i)$ is the detection flag, i.e.,

$$\theta_{\mathrm{D}}(\boldsymbol{a}_k^i) = \begin{cases} 0 & \forall j,\ a_k^{i,j} = 0 \\ 1 & \text{otherwise} \end{cases} \tag{18}$$

In order to factorize the factor node,[12] corresponding to $\varphi(\boldsymbol{A}_k)$ in factor graph, $\boldsymbol{B}_k$ is used and the indicator function is obtained by

$$\varphi(\boldsymbol{A}_k, \boldsymbol{B}_k) = \prod_{i=1}^{n_k} \prod_{j=1}^{m_k} \varphi(\boldsymbol{a}_k^i, b_k^j) \tag{19}$$

where

$$\varphi(\mathbf{a}_k^i, b_k^j) = \begin{cases} 0 & \text{if } a_k^{i,j} = 1,\ b_k^j \neq i \text{ or if } b_k^j = i,\ a_k^{i,j} \neq 1 \\ 1 & \text{otherwise} \end{cases} \tag{20}$$

Thus,

$$f(\boldsymbol{A}_k|\boldsymbol{\xi}_k)=\prod_{i=1}^{n_k}\left\{P_{\mathrm{D}}\left(\boldsymbol{\xi}_k^i\right)^{\theta_{\mathrm{D}}\left(\boldsymbol{a}_k^i\right)}\left[1-P_{\mathrm{D}}\left(\boldsymbol{\xi}_k^i\right)\right]^{1-\theta_{\mathrm{D}}\left(\boldsymbol{a}_k^i\right)}\prod_{j=1}^{m_k}\varphi\left(\boldsymbol{a}_k^i,b_k^j\right)\right\} \tag{21}$$

Furthermore, the PDF of $\boldsymbol{Z}_k$ conditioned on $\boldsymbol{\xi}_k$ and $\boldsymbol{A}_k$ is defined as

$$f(\boldsymbol{Z}_k|\boldsymbol{\xi}_k,\boldsymbol{A}_k)=\prod_{i=1}^{n_k}f\left(\boldsymbol{Z}_k^{\boldsymbol{a}_k^i}|\boldsymbol{\xi}_k^i\right)^{\theta_{\mathrm{D}}\left(\boldsymbol{a}_k^i\right)}\prod_{j|b_k^j=0}\lambda_{\mathrm{fan}}\left(\boldsymbol{z}_k^j\right) \tag{22}$$

where $\boldsymbol{Z}_k^{\boldsymbol{a}_k^i}$ is the measurement cell corresponding to $\boldsymbol{a}_k^i$. Based on Eq. (21) and Eq. (22), the joint PDF of $\boldsymbol{Z}_k$ and $\boldsymbol{A}_k$ conditioned on $\boldsymbol{\xi}_k$ is given by

$$\begin{aligned}f(\boldsymbol{Z}_k,\boldsymbol{A}_k|\boldsymbol{\xi}_k)&=f(\boldsymbol{Z}_k|\boldsymbol{\xi}_k,\boldsymbol{A}_k)f(\boldsymbol{A}_k|\boldsymbol{\xi}_k)\\&=\prod_{i=1}^{n_k}\left\{\left[P_{\mathrm{D}}\left(\boldsymbol{\xi}_k^i\right)f\left(\boldsymbol{Z}_k^{\boldsymbol{a}_k^i}|\boldsymbol{\xi}_k^i\right)\right]^{\theta_{\mathrm{D}}\left(\boldsymbol{a}_k^i\right)}\right.\\&\left.\times\left[1-P_{\mathrm{D}}\left(\boldsymbol{\xi}_k^i\right)\right]^{1-\theta_{\mathrm{D}}\left(\boldsymbol{a}_k^i\right)}\prod_{j=1}^{m_k}\varphi\left(\boldsymbol{a}_k^i,b_k^j\right)\right\}\prod_{j|b_k^j=0}\lambda_{\mathrm{fan}}\left(\boldsymbol{z}_k^j\right)\end{aligned} \tag{23}$$

Furthermore, the joint posterior PDF of targets and associations is obtained by

$$\begin{aligned}\overset{>}{f}(\boldsymbol{\xi}_k,\boldsymbol{A}_k|\boldsymbol{Z}^k)&\propto f(\boldsymbol{\xi}_k|\boldsymbol{Z}^{k-1})f(\boldsymbol{Z}_k,\boldsymbol{A}_k|\boldsymbol{\xi}_k)\\&=\prod_{i=1}^{n_k}\left\{f(\boldsymbol{\xi}_k^i|\boldsymbol{Z}^{k-1})\left[P_{\mathrm{D}}\left(\boldsymbol{\xi}_k^i\right)f\left(\boldsymbol{Z}_k^{\boldsymbol{a}_k^i}|\boldsymbol{\xi}_k^i\right)\right]^{\theta_{\mathrm{D}}\left(\boldsymbol{a}_k^i\right)}\right.\\&\left.\left(1-P_{\mathrm{D}}\left(\boldsymbol{\xi}_k^i\right)\right)^{1-\theta_{\mathrm{D}}\left(\boldsymbol{a}_k^i\right)}\prod_{j=1}^{m_k}\varphi\left(\boldsymbol{a}_k^i,b_k^j\right)\right\}\prod_{j|b_k^j=0}\lambda_{\mathrm{fan}}\left(\boldsymbol{z}_k^j\right)\end{aligned} \tag{24}$$

3.2. LBP based extended target tracking

The goal of data association is calculating the joint posterior PDF of association variables, referred to as $f\left(\boldsymbol{a}_k^i|\boldsymbol{Z}^k\right)$, which can be approximated by marginalizing the joint posterior PDF in Eq. (24). The joint posterior PDF is described by the factor graph in Fig. 1 where variable nodes and factor nodes are represented by circles and squares, respectively. Then, the data association problem can be solved by the LBP algorithm. According to Eq. (24), the message from the factor node $\varphi_i\left(\boldsymbol{\xi}_k^i,\boldsymbol{a}_k^i\right)$ to the variable node $\boldsymbol{a}_k^i$ can be given by

$$\alpha_k^i\left(\boldsymbol{a}_k^i\right)=\int\varphi_i\left(\xi_k^i,\boldsymbol{a}_k^i\right)f\left(\boldsymbol{\xi}_k^i|\boldsymbol{Z}^{k-1}\right)\mathrm{d}\boldsymbol{\xi}_k^i \tag{25}$$

where

$\varphi_i\left(\boldsymbol{\xi}_k^i,\boldsymbol{a}_k^i\right)=\left[P_{\mathrm{D}}\left(\boldsymbol{\xi}_k^i\right)f\left(\boldsymbol{Z}_k^{\boldsymbol{a}_k^i}|\boldsymbol{\xi}_k^i\right)\right]^{\theta_{\mathrm{D}}\left(\boldsymbol{a}_k^i\right)}\left[1-P_{\mathrm{D}}\left(\boldsymbol{\xi}_k^i\right)\right]^{1-\theta_{\mathrm{D}}\left(\boldsymbol{a}_k^i\right)}$. The message from the factor h_j to the variable node b_k^i is $\beta_k^j\left(b_k^j\right)$, i.e.,

$$\beta_k^j\left(b_k^j\right)=\begin{cases}\lambda_{\mathrm{fan}}\left(\boldsymbol{z}_k^j\right) & b_k^j=0\\ 1 & b_k^j\neq 0\end{cases} \tag{26}$$

Once $\alpha_k^i\left(\boldsymbol{a}_k^i\right)$ and $\beta_k^j\left(b_k^j\right)$ are obtained, the lth message passing iteration, involving the factor nodes $\varphi\left(\boldsymbol{a}_k^i,b_k^j\right)$ and the variable nodes $\boldsymbol{a}_k^i$ and b_k^j, is performed by calculating the message from the factor node $\varphi\left(\boldsymbol{a}_k^i,b_k^j\right)$ to the variable node b_k^j, denoted by $\mu_{i\to j}^l\left(b_k^j\right)$, and the message from the factor node $\varphi\left(\boldsymbol{a}_k^i,b_k^j\right)$ to the variable node $\boldsymbol{a}_k^i$, denoted by $\upsilon_{j\to i}^l\left(\boldsymbol{a}_k^i\right)$. $\mu_{i\to j}^l\left(b_k^j\right)$ and $\upsilon_{j\to i}^l\left(\boldsymbol{a}_k^i\right)$ are calculated by

$$\mu_{i\to j}^l\left(b_k^j\right)=\sum_{\boldsymbol{a}_k^i\in\mathcal{A}}\left[\varphi\left(\boldsymbol{a}_k^i,b_k^j\right)\alpha_k^i\left(\boldsymbol{a}_k^i\right)\prod_{j'=1|j'\neq j}^{m_k}\upsilon_{j'\to i}^l\left(\boldsymbol{a}_k^i\right)\right] \tag{27}$$

$$\upsilon_{j\to i}^l\left(\boldsymbol{a}_k^i\right)=\sum_{b_k^j=0}^{n_k}\left[\varphi\left(\boldsymbol{a}_k^i,b_k^j\right)\beta_k^j\left(b_k^j\right)\prod_{i'=1|i'\neq i}^{n_k}\mu_{i'\to j}^{l-1}\left(b_k^i\right)\right] \tag{28}$$

In each iteration, the number of μ and υ are $n_k^2m_k$ and $2^{m_k}n_km_k$, respectively. There are $2^{m_k}-1$ additions in calculating $\mu_{i\to j}^l\left(b_k^j\right)$ as Eq. (27). Each component of the additions needs m_k multiplications. There are n_k additions in calculating $\upsilon_{j\to i}^l\left(\boldsymbol{a}_k^i\right)$ as Eq. (28). Each component of the additions needs n_k multiplications. As a consequence, the complexity per iteration is $O\left(2^{m_k}m_k^2n_k^2+2^{m_k}n_k^3m_k\right)$. Note that the massage passing iteration is of high computational burden. The message $\mu_{i\to j}^l\left(b_k^j\right)$ takes the same value when $b_k^j\neq i$, and they can be normalized as 1. Thus, $\mu_{i\to j}^l\left(b_k^j\right)$ can be simplified as

$$\mu_{i\to j}^l(i)=\frac{\sum_{\boldsymbol{a}_k^i\in\mathcal{A}|a_k^{i,j}=1}\left[\alpha_k^i\left(\boldsymbol{a}_k^i\right)\prod_{j'=1|a_k^{i,j'}=1,j'\neq j}^{m_k}\upsilon_{j'\to i}^l\left(\boldsymbol{a}_k^i\right)\right]}{\alpha_k^i(0)+\sum_{\boldsymbol{a}_k^i\in\mathcal{A}|a_k^{i,j}=0,\boldsymbol{a}_k^i\neq\boldsymbol{0}}\alpha_k^i\left(\boldsymbol{a}_k^i\right)\prod_{j'=1|a_k^{i,j'}=1,j'\neq j}^{m_k}\upsilon_{j'\to i}^l\left(\boldsymbol{a}_k^i\right)} \tag{29}$$

At the same time, $\upsilon_{j\to i}^l\left(\boldsymbol{a}_k^i\right)$ takes the same value when $a_k^{i,j}=0$, and they can be normalized as 1. Thus, $\upsilon_{j\to i}^l\left(\boldsymbol{a}_k^i\right)$ can also be simplified as

$$\upsilon_{j\to i}^l\left(\boldsymbol{a}_k^{i^*}\right)=\frac{\beta_k^j(i)}{\beta_k^j(0)+\sum_{i'=1|i'\neq i}^{n_k}\beta_k^j(i')\mu_{i'\to j}^{l-1}(i')} \tag{30}$$

where $\boldsymbol{a}_k^{i^*}\in\left\{\boldsymbol{a}_k^i|a_k^{i,j}=1\right\}$ for a given j. Different from Eq. (27) and Eq. (28), the number of μ is reduced to n_km_k and the number of υ is $2^{m_k-1}n_km_k$ at most in each iteration. There are $2^{m_k}-1$ additions and one division in calculating $\mu_{i\to j}^l(i)$ as Eq. (29). Each component of the additions needs m_k multipli-

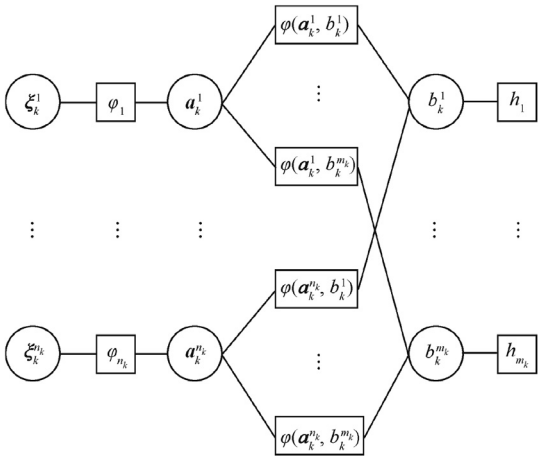

Fig. 1 Factor graph for data association problem in METT.

cations at most. There are n_k additions and one division in calculating $\upsilon_{j\to i}^{l}(\boldsymbol{a}_k^{i^*})$ as Eq. (30). Each component of the additions needs one multiplication at most. As a consequence, the complexity per iteration is $O\left(2^{m_k}m_k^2n_k+2^{m_k}n_k^2m_k\right)$ at most.

When the iterative algorithm is converged until the l^*th iteration, approximations of the marginal posterior distribution $f(\boldsymbol{a}_k^i|\boldsymbol{Z}^k)$ are calculated by

$$\hat{f}(\boldsymbol{a}_k^i|\boldsymbol{Z}^k)=\frac{\alpha(\boldsymbol{a}_k^i)\prod_{j=1}^{m_k}\upsilon_{j\to i}^{l^*}(\boldsymbol{a}_k^i)}{\sum_{\boldsymbol{a}'^i_k\in\mathcal{A}}\alpha(\boldsymbol{a}'^i_k)\prod_{j=1}^{m_k}\upsilon_{j\to i}^{l^*}(\boldsymbol{a}'^i_k)} \tag{31}$$

$$\hat{f}(b_k^j=i|\boldsymbol{Z}^k)=\frac{\beta_k^j(i)\mu_{i\to j}^{l^*}(i)}{\sum_{i'=1}^{n_k}\beta_k^j(i')\mu_{i'\to j}^{l^*}(i')} \tag{32}$$

The relationship between Eq.(31) and Eq.(32) is given by Property 1.

Property 1. $\hat{f}(b_k^j|\boldsymbol{Z}^k)$ in Eq. (32) can be approximated according to $\hat{f}(\boldsymbol{a}_k^i|\boldsymbol{Z}^k)$ in Eq. (31) as

$$\hat{f}(b_k^j=i|\boldsymbol{Z}^k)\approx\frac{1+\mu_{i\to j}(i)}{\sum_{i'}\mu_{i'\to j}(i)}\sum_{\boldsymbol{a}_k^i\in\mathcal{A}|a_k^{i,j}=1}\hat{f}(\boldsymbol{a}_k^i|\boldsymbol{Z}^k)\qquad b_k^j>0 \tag{33}$$

Proof. According to Assumption (4), $\lambda_{\text{fan}}(\boldsymbol{z}_k^j)=\lambda_{\text{fan}}$. Reformulating Eq. (24) by dividing $\lambda_{\text{fan}}^{m_k}$, $\alpha_k^i(\boldsymbol{a}_k^i)$ and $\beta_k^j(b_k^j)$ can be given as

$$\alpha_k^i(\boldsymbol{a}_k^i)=\frac{\int\varphi_i(\boldsymbol{\xi}_k^i,\boldsymbol{a}_k^i)f(\boldsymbol{\xi}_k^i|\boldsymbol{Z}^{k-1})\mathrm{d}\boldsymbol{\xi}_k^i}{\lambda_{\text{fan}}^{\sum_j a_k^{i,j}}} \tag{34}$$

and

$$\beta_k^j(b_k^j)=1 \tag{35}$$

Then, using Eq. (29) and Eq. (32), we have

$$\begin{aligned}\hat{f}(b_k^j=i|\boldsymbol{Z}^k)&=\frac{\mu_{i\to j}(i)}{\sum_{i'=1}^{n_k}\mu_{i'\to j}(i')}=\frac{\sum_{\boldsymbol{a}_k^i\in\mathcal{A}|a_k^{i,j}=1}\left[\alpha_k^i(\boldsymbol{a}_k^i)\prod_{j'=1|a_k^{i,j'}=1,j'\neq j}^{m_k}\upsilon_{j'\to i}^{l}(\boldsymbol{a}_k^i)\right]}{\sum_{i'=1}^{n_k}\mu_{i'\to j}(i')}\\&=\frac{\sum_{\boldsymbol{a}_k^i\in\mathcal{A}|a_k^{i,j}=1}\left[\alpha_k^i(\boldsymbol{a}_k^i)\prod_{j'=1|a_k^{i,j'}=1,j'\neq j}^{m_k}\upsilon_{j'\to i}^{l}(\boldsymbol{a}_k^i)\right]}{\sum_{\boldsymbol{a}_k^i\in\mathcal{A}}\left[\alpha_k^i(\boldsymbol{a}_k^i)\prod_{j'=1|a_k^{i,j'}=1,j'\neq j}^{m_k}\upsilon_{j'\to i}^{l}(\boldsymbol{a}_k^i)\right]}\cdot\frac{\sum_{\boldsymbol{a}_k^i\in\mathcal{A}|a_k^{i,j}=1}\left[\alpha_k^i(\boldsymbol{a}_k^i)\prod_{j'=1|a_k^{i,j'}=1,j'\neq j}^{m_k}\upsilon_{j'\to i}^{l}(\boldsymbol{a}_k^i)\right]}{\sum_{\boldsymbol{a}_k^i\in\mathcal{A}|a_k^{i,j}=0}\left[\alpha_k^i(\boldsymbol{a}_k^i)\prod_{j'=1|a_k^{i,j'}=1,j'\neq j}^{m_k}\upsilon_{j'\to i}^{l}(\boldsymbol{a}_k^i)\right]}\cdot\frac{\sum_{\boldsymbol{a}_k^i\in\mathcal{A}}\left[\alpha_k^i(\boldsymbol{a}_k^i)\prod_{j'=1|a_k^{i,j'}=1,j'\neq j}^{m_k}\upsilon_{j'\to i}^{l}(\boldsymbol{a}_k^i)\right]}{\sum_{i'=1}^{n_k}\mu_{i'\to j}(i')}\\&=\frac{1+\mu_{i\to j}(i)}{\sum_{i'=1}^{n_k}\mu_{i'\to j}(i')}\sum_{\boldsymbol{a}_k^i|a_k^{i,j}=1}\frac{\alpha_k^i(\boldsymbol{a}_k^i)\prod_{j'=1|a_k^{i,j'}=1,j'\neq j}^{m_k}\upsilon_{j'\to i}^{l}(\boldsymbol{a}_k^i)}{\sum_{\boldsymbol{a}_k^i\in\mathcal{A}}\left[\alpha_k^i(\boldsymbol{a}_k^i)\prod_{j'=1|a_k^{i,j'}=1,j'\neq j}^{m_k}\upsilon_{j'\to i}^{l}(\boldsymbol{a}_k^i)\right]}\approx\frac{1+\mu_{i\to j}(i)}{\sum_{i'=1}^{n_k}\mu_{i'\to j}(i')}\sum_{\boldsymbol{a}_k^i\in\mathcal{A}|a_k^{i,j}=1}\hat{f}(\boldsymbol{a}_k^i|\boldsymbol{Z}^k)\end{aligned} \tag{36}$$

In the proof, $\hat{f}(\boldsymbol{a}_k^i|\boldsymbol{Z}^k)$ is approximated by $\alpha_k^i(\boldsymbol{a}_k^i)\prod_{j'=1|a_k^{i,j'}=1,j'\neq j}^{m_k}\upsilon_{j'\to i}^{l}(\boldsymbol{a}_k^i)/\sum_{\boldsymbol{a}_k^i\in\mathcal{A}}\left[\alpha_k^i(\boldsymbol{a}_k^i)\prod_{j'=1|a_k^{i,j'}=1,j'\neq j}^{m_k}\upsilon_{j'\to i}^{l}(\boldsymbol{a}_k^i)\right]$. The reason for this is that $\upsilon_{j\to i}^{l}(\mathbf{a}_k^i)$ is 1 when $a_k^{i,j}=0$. If measurement j is generated by target i, $\mu_{i\to j}(i)$ is generally with big value in Eq. (29), because $\alpha_k^i(\boldsymbol{a}_k^i)(\boldsymbol{a}_k^i\in\{\boldsymbol{a}_k^i|a_k^{i,j}=1\})$ are with big values. Thus, $\upsilon_{j\to i}(\boldsymbol{a}_k^i)(\boldsymbol{a}_k^i\in\{\boldsymbol{a}_k^i|a_k^{i,j}=1\})$ in Eq. (30) are generally close to 1 because the denominator does not contain $\mu_{i\to j}(i)$. If measurement j is not generated by target i, it can also be seen that $\alpha_k^i(\boldsymbol{a}_k^i)$ and $\upsilon_{j\to i}(\boldsymbol{a}_k^i)(\boldsymbol{a}_k^i\in\{\boldsymbol{a}_k^i|a_k^{i,j}=1\})$ are with small values. Therefore, the approximation is reasonable.

The convergence of the loopy max-product BP algorithm has been proved.[34] Although the convergence cannot be extended to the sum-product BP algorithm, the LBP algorithm has good performance in many applications and the advantages of the LBP algorithm will be demonstrated in the simulations of Section 4.

3.3. Difference between ET-LBP and ET-BP

3.3.1. Tracking accuracy

In the ET-BP algorithm, $\hat{f}(\boldsymbol{a}_k^i|\boldsymbol{Z}^k)$ depends on $\prod_{f\in v_i}u_{f\to i}(\boldsymbol{a}_k^i)$, where these factor nodes in v_i only guarantee that the measurement cell associated with target i has no conflict with that of other targets. However, this measurement cell may be with too few measurements. Such drawback results in a significant deviation of the extension state estimation. Different from the ET-BP algorithm, $\hat{f}(\boldsymbol{a}_k^i|\boldsymbol{Z}^k)$ in the ET-LBP algorithm depends on $\prod_{j=1}^{m_k}\upsilon_{j\to i}(\boldsymbol{a}_k^i)$, where these m_k factor nodes contain the information of all measurements at time k. If the target i is associated with too many or too few measurements, $\prod_{j=1}^{m_k}\upsilon_{j\to i}(\boldsymbol{a}_k^i)$ will be with small value. Furthermore, Property 1 shows that $\hat{f}(b_k^j|\boldsymbol{Z}^k)$ is related to all $\hat{f}(\boldsymbol{a}_k^i|\boldsymbol{Z}^k)$ with $a_k^{i,j}=1$, as seen in Eq. (33), which means that $\hat{f}(b_k^j|\boldsymbol{Z}^k)$ considers the information of all measurement cells containing the measurement j. Thus, it can avoid the drawback mentioned in the ET-BP algorithm.

3.3.2. Computational complexity

In the ET-BP algorithm, the factor node $\varphi(\boldsymbol{a}_k^i,\boldsymbol{a}_k^j)$ of the joint posterior PDF is defined over two variables $\boldsymbol{a}_k^i$ and $\boldsymbol{a}_k^j$. It is complex that the factor node has $(2^{m_k})^2$ values. The ET-LBP algorithm is more efficient than the ET-BP algorithm, because the factor node $\varphi(\boldsymbol{a}_k^i,b_k^j)$ in the ET-LBP algorithm has only $2^{m_k}m_k$ values. Meanwhile, the graphical model of the ET-LBP algorithm, as shown in Fig. 1, has better performance than that of the ET-BP algorithm. The reason for this is that all association variables are connected to each other in the model of the ET-BP algorithm, resulting in higher computational complexity.

Additionally, since an extended target can generate one or more than one measurement per time step, all measurement cells should be considered in extended target tracking. The ET-LBP algorithm avoids extra computation on all measurement cells, compared with the ET-BP algorithm. In each iteration of the ET-BP algorithm, the numbers of $u_{n\to f}$ and $u_{f\to n}$ are $2^{m_k}n_k^2$. There are n_k-1 multiplications in calculating

$u_{n\to f}(x_n)$ in Eq. (9), and 2^{m_k} additions in calculating $u_{f\to n}(x_n)$ in Eq. (10). Each component of the additions contains one multiplication. As a consequence, the complexity of the ET-BP algorithm per iteration is $O\left((2^{m_k})^2 n_k^2 + 2^{m_k} n_k^3\right)$. It can be seen that the complexity of the ET-LBP algorithm is lower than that of the ET-BP algorithm, because the complexity of the ET-BP algorithm is proportional to $(2^{m_k})^2$.

3.4. Improved SMS

Although Eq. (29) and Eq. (30) are more efficient than Eq. (27) and Eq. (28), they involve all possible $\boldsymbol{a}_k^i$. It is intractable because the number of all possible $\boldsymbol{a}_k^i$ increases with the size of $\boldsymbol{Z}_k$ rapidly. Most of $\boldsymbol{a}_k^i$ have small $f\left(\boldsymbol{Z}_k^{\boldsymbol{a}_k^i}|\boldsymbol{\xi}_k^i\right)$. These small values can be neglected due to the corresponding small $\alpha_k^i(\boldsymbol{a}_k^i)$. Thus, it is necessary to decrease the computational burden by truncating $\boldsymbol{a}_k^i$ with small $f\left(\boldsymbol{Z}_k^{\boldsymbol{a}_k^i}|\boldsymbol{\xi}_k^i\right)$.

It has been shown that the measurement $\boldsymbol{Z}_k$ can be approximated by the SMS based on Minimal Spanning Tree (MST) algorithm[20]. The measurements, close to each other, are considered as generating from the same extended target in the SMS. Simulations based on random matrices show that the SMS is insufficient when some extended targets are close in space. This phenomenon is similar to the insufficiency of distance partition[5]. The SMS with thresholds cannot distinguish measurements of two extended targets well when they are close in space. It may result in $\boldsymbol{a}_k^i$ with too many or too less measurements. Thus, the wrong measurement association may cause a significant error in extension state estimation.

Fig. 2 explains phenomenon using an example. In Fig. 2(a), two extended targets are denoted in solid ellipses, and the measurements of these two extended targets are denoted in points. The SMS with threshold is shown in Fig. 2(b), where measurement cells are denoted in dotted ellipses. It can be seen that the left measurement cell contains measurements of the right extended target. The reason for this is that several measurements of the right target are close to the left target. Consequently, the left measurement cell is with too many measurements, and the right measurement cell is with too few measurements.

In order to handle this phenomenon, an Improved SMS (ISMS) is proposed based on the prediction information. On the one hand, the K best associations of each target are added in the SMS. On the other hand, the subpartition for big measurement cells is also considered. The K best associations and the subpartition are given as follows.

3.4.1. K best associations

Consider the ith target with kinematic state $\boldsymbol{x}_k^i$, extension state $\boldsymbol{X}_k^i$ and likelihood function $f\left(\boldsymbol{Z}_k^{\boldsymbol{a}_k^i}|\boldsymbol{\xi}_k^i\right)$, where $\boldsymbol{Z}_k^{\boldsymbol{a}_k^i}$ are measurements associated with target i. $\boldsymbol{a}_k^i$ with high $f\left(\boldsymbol{Z}_k^{\boldsymbol{a}_k^i}|\boldsymbol{\xi}_k^i\right)$ can be selected without exhaustively considering all possible $\boldsymbol{a}_k^i$. This can be accomplished by computing the K best associations of target i. Then, the likelihood function[24] of target i can be expressed as

$$\begin{aligned} f\left(\boldsymbol{Z}_k^{\boldsymbol{a}_k^i}|\boldsymbol{\xi}_k^i\right) &= f\left(\boldsymbol{Z}_k^{\boldsymbol{a}_k^i}, m_k^{\boldsymbol{a}_k^i}|\boldsymbol{\xi}_k^i\right) \\ &= f\left(m_k^{\boldsymbol{a}_k^i}|\gamma_k^i\right) f\left(\boldsymbol{Z}_k^{\boldsymbol{a}_k^i}|\boldsymbol{x}_k^i, \boldsymbol{X}_k^i\right) \\ &= \mathcal{P}\left(m_k^{\boldsymbol{a}_k^i}|\gamma_k^i\right) \prod_{j|a_k^{ij}=1} \mathcal{N}\left(\boldsymbol{z}_k^j; \boldsymbol{x}_k^i, \boldsymbol{X}_k^i\right) \end{aligned} \tag{37}$$

where $m_k^{\boldsymbol{a}_k^i}$ is the number of measurements in $\boldsymbol{Z}_k^{\boldsymbol{a}_k^i}$, and $\mathcal{P}(n|\gamma)$ denotes a Poisson distribution defined over the variable n with rate γ. In order to compute the K best association of target i, a ranking scheme of all $\boldsymbol{a}_k^i$ based on $f\left(\boldsymbol{Z}_k^{\boldsymbol{a}_k^i}|\boldsymbol{\xi}_k^i\right)$ is needed. Once the number of measurements is fixed in Eq.(37), Murty's algorithm[35] can be used to compute the K best associations of target i where the cost vector is constructed as $\boldsymbol{C}_k^i = \left[\mathcal{N}\left(\boldsymbol{z}_k^1; \boldsymbol{x}_k^i, \boldsymbol{X}_k^i\right), \mathcal{N}\left(\boldsymbol{z}_k^2; \boldsymbol{x}_k^i, \boldsymbol{X}_k^i\right), \ldots, \mathcal{N}\left(\boldsymbol{z}_k^{m_k}; \boldsymbol{x}_k^i, \boldsymbol{X}_k^i\right)\right]$. But, the K best associations of target i should consider all possible measurement numbers. The procedure of computing the K best associations of target i based on Murty's algorithm is illustrated in Table 2.

3.4.2. Subpartition

When targets are close in space, there may exist measurement cells with too many measurements in the SMS with thresholds.[20] This is because measurements from more than one target will be assigned to the same measurement cell. Such measurement cells would make some targets associate with too many measurements. Therefore, the tracking accuracy is poor in this situation. A subpartition algorithm[6] has been proposed based on K-means clustering. It can split these measure-

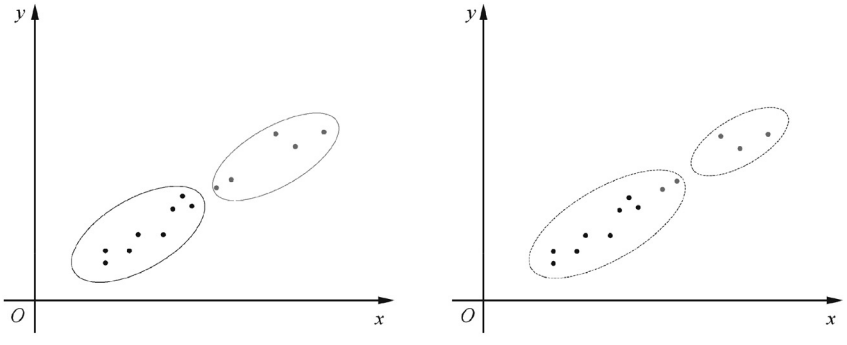

(a) True measurement (b) Measurement cell in SMS

Fig. 2 Factor graph for data association problem in METT.

Table 2 Computing the K best associations of target i

Input: K, $\boldsymbol{Z}_k$, $f\left(\boldsymbol{Z}_k^{a_k^i}|\boldsymbol{\xi}_k^i\right)$ for arbitrary $\boldsymbol{a}_k^i$;
Output: $\mathcal{W}$;
$n=1$;
$\mathcal{W}=\phi$;
For $j=1:m_k$
  L_j is the maximum likelihood of association when target i is associated with j measurements;
  w_j is the measurement index corresponding to L_j;
End
While $n \leqslant K$
  Find the maximum of $\{L_j\}_{j=1}^{m_k}$ denoted by L_{j^*};
  $\mathcal{W}=\mathcal{W}\oplus w_{j^*}$;
  Single stage operation of Murty's algorithm[35] is performed to update L_{j^*} and w_{j^*};
  $n=n+1$;
End

ment cells, with too many measurements, into smaller cells. In order to avoid such a situation in the SMS, measurement cells generated by subpartition are added into the SMS.

Remark. The ISMS is composed of three parts, including the measurement cells from the SMS, the K best associations and the subpartition. It is worth noting that using all these three parts in this work is essential. The SMS contains measurement cells, which are most likely generated from extended targets. Because the SMS is not accurate when targets are close in space, the measurement cells from the K best associations and the subpartition are needed. Besides, the K best associations rely on prediction information. It may return non-informative measurement cells when targets are maneuvering. Thus, only the measurement cells from the K best associations are not enough. For this reason, it is better to use all these three parts.

4. Simulations

In this section, the ET-LBP algorithm is compared with the algorithms[20] based on the SMS, named ET-BP-SMS and JPDA-SMS. In order to verify the effectiveness of the proposed algorithm, the SMS[20] and the ISMS in Section 3.4 are used in the proposed algorithm, named ET-LBP-SMS and ET-LBP-ISMS, respectively.

4.1. Parameter setting

Two challenging scenarios are used to verify the performance of the proposed algorithm. The actual trajectories are shown in Fig. 3, where the trajectories are denoted by ellipses, and the measurements are denoted by points. 101 time steps are simulated in the surveillance area $[-500,500]\,\mathrm{m}\times[-300,300]\,\mathrm{m}$. The major and minor axes of the target trajectory ellipses are set to be 10 m and 5 m, respectively. In the first scenario, as shown in Fig. 3(a), three targets move closely, starting at $(-500,-50)$ m, $(-500,0)$ m and $(-500,50)$ m, respectively. In the second scenario, as shown in Fig. 3(b), two targets move closer before separating. The minimum target separation is 50 m. The parameters of the motion model are set to be $T_\mathrm{s}=1$ s, $\boldsymbol{\Sigma}=0.1\ \mathrm{m/s^2}$, $\theta=1$ s and $\tau=5$ s. The measurement rates, clutter intensity and validation gate of each target are set to be 10, 1.3×10^{-5} and 150 m, respectively. The upper probability P_U and lower probability P_L are set to be 0.7 and 0.3, respectively. The maximum number of iterations is set to be 50 in the LBP and BP algorithms. In this work, the cases with $P_\mathrm{D}(\boldsymbol{\xi})\in\{0.99,0.80\}$ are considered. 500 Monte Carlo simulations are performed in the experiments.

In order to evaluate the performance of these algorithms, the evaluation criteria[20] are used. The Tracking Success Rate (TSR) is used to evaluate the performance of these algorithms and defined as

$$\mathrm{TSR}=V/C \tag{38}$$

where V and C are the number of trials without tracking lost and the total number of Monte Carlo trials, respectively. The distance between the kinematic state $\boldsymbol{x}_k^i$ and $\boldsymbol{x}_k^j$ is defined as

$$d_{i,j}^{\boldsymbol{x}}=\|\boldsymbol{x}_k^i-\boldsymbol{x}_k^j\|_2 \tag{39}$$

and the distance between the extension state $\boldsymbol{X}_k^i$ and $\boldsymbol{X}_k^j$ is defined as

$$d_{i,j}^{\boldsymbol{X}}=\|\boldsymbol{X}_k^i-\boldsymbol{X}_k^j\|_\mathrm{F} \tag{40}$$

where $\|\cdot\|_2$ and $\|\cdot\|_\mathrm{F}$ are the Euclidean norm and Frobenius norm, respectively.

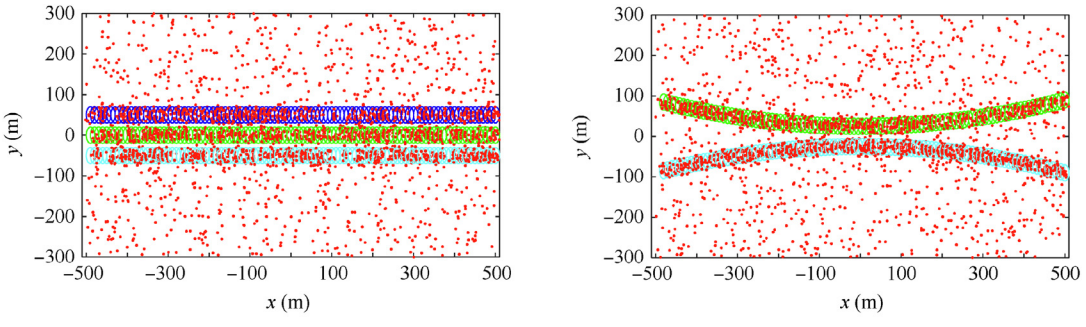

(a) Scenario one (b) Scenario two

Fig. 3 True target trajectories when $P_\mathrm{D}=0.99$.

4.2. Simulation results

4.2.1. Scenario one

The simulations are performed by MATLAB R2015b on PC with Intel Core i3-7100 3.90 GHz processor and 8 GB RAM. The proposed algorithm is simulated in terms of tracking accuracy, computational efficiency and convergence.

In case of $P_D = 0.99$, the TSRs of the ET-LBP-ISMS, ET-LBP-SMS, ET-BP-SMS and JPDA-SMS algorithms are 97.4%, 96.2%, 96.4% and 94.6%, respectively. It can be seen that the ET-LBP-ISMS algorithm is better than the other algorithms in TSR, and that the ET-LBP-SMS and ET-BP-SMS algorithms almost have the same performance. The position error and extension error of these algorithms are shown in Fig. 4 when $P_D = 0.99$. From Fig. 4(a), it can be seen that the ET-LBP-ISMS algorithm has a smaller error in position estimation. The reason for this is that the ISMS considers the prediction information and includes the subpartition operation. The ET-LBP-SMS, ET-BP-SMS and JPDA-SMS algorithms are all based on the SMS. Although the ET-LBP-SMS algorithm almost has the same performance with the ET-BP-SMS and the JPDA-SMS algorithms in position estimation, it has a more accurate extension state estimation, as seen in Fig. 4(b). The main flaw of the ET-BP-SMS algorithm is the deviation in extension state estimation, compared with the JPDA-SMS algorithm. Thus, the ET-LBP-SMS algorithm overcomes the flaw in the ET-BP-SMS algorithm with better efficiency, which is consistent with the analysis results in Section 3.3.1.

In case of $P_D = 0.80$, the TSRs of the ET-LBP-ISMS, ET-LBP-SMS, ET-BP-SMS and JPDA-SMS algorithms are 96.0%, 94.4%, 95.6% and 91.6%, respectively. The position error and extension error of these algorithms are shown in Fig. 5 when $P_D = 0.80$. Although all these algorithms have larger errors in position and extension state estimation with lower P_D, they can track targets well. Therefore, the proposed algorithms are robust to lower P_D.

Simulations show that the performance of the ET-BP-SMS algorithm is sensitive to the upper probability and lower probability. In the precious algorithm,[20] the upper probability and lower probability are set to be 0.6 and 0.4, respectively. Thus, the number of measurement cells in the SMS is small, and the run time of the ET-BP-SMS algorithm is shorter. The SMS used in this paper contains more measurement cells. The extension error becomes larger in this paper because the wrong measurement cells in the new measurement cells influence the

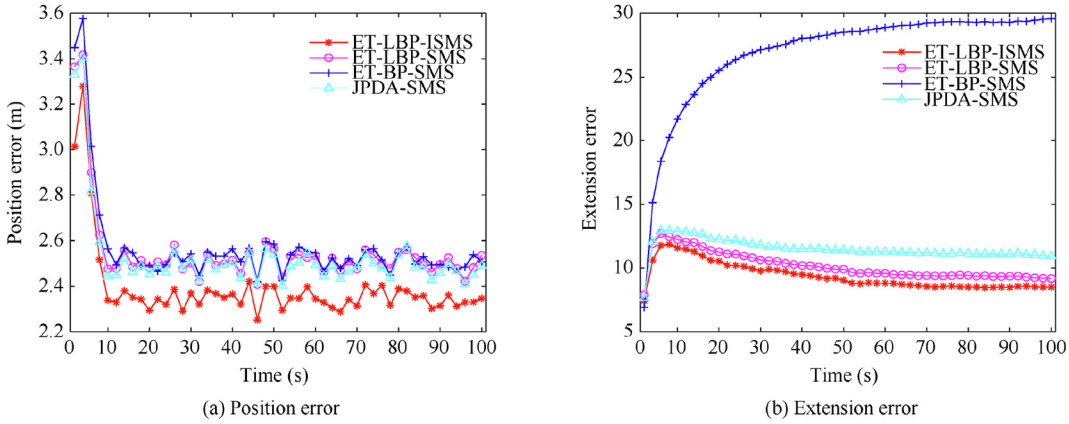

Fig. 4 Position error and extension error of ET-LBP-ISMS, ET-LBP-SMS, ET-BP-SMS and JPDA-SMS algorithms in scenario one when $P_D = 0.99$.

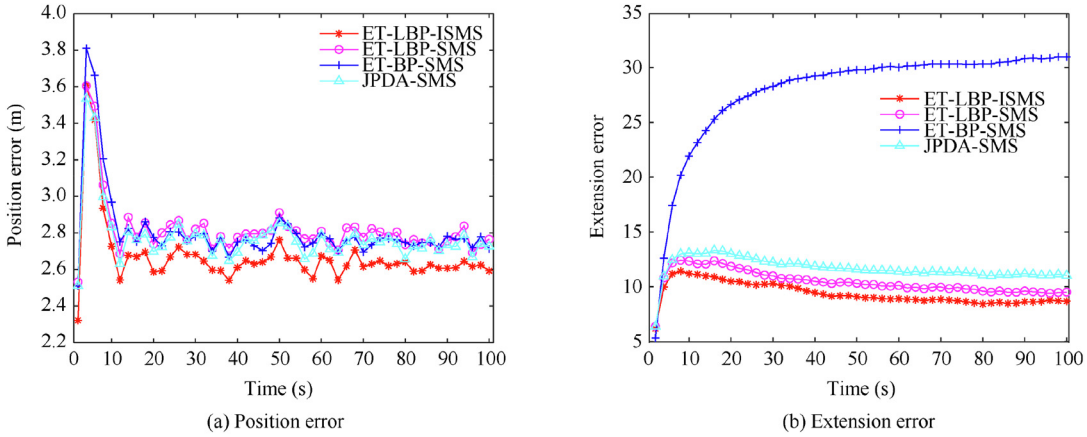

Fig. 5 Position error and extension error of ET-LBP-ISMS, ET-LBP-SMS, ET-BP-SMS and JPDA-SMS algorithms in scenario one when $P_D = 0.80$.

performance of the ET-BP-SMS algorithm. It can be seen that the ET-LBP-SMS algorithm is more robust to the upper probability and lower probability of the SMS.

At time step k, suppose that the numbers of targets and measurements are n_k and m_k while the numbers of measurement cells in SMS and ISMS are N_1 and N_2. Because the JPDA for extended target tracking enumerates all possible events, the complexity is $O\left(n_k^{2^{m_k}}\right)$. It can be seen that the complexity of the ET-LBP algorithm is lower than that of JPDA for extended target tracking since JPDA includes a combinatorial explosion. At the same time, the SMS is based on the Prim algorithm, in which the complexity is $O\left(n_k^2\right)$. The ISMS is based on the Prim algorithm and K best algorithm in which the complexity is $O\left(n_k^2 + Kn_k m_k^2\right)$. With the SMS or ISMS, the number of measurement cells can be reduced from 2^{m_k} to N_1 or N_2. Therefore, the complexity of ET-LBP-ISMS, ET-LBP-SMS, ET-BP-SMS and JPDA-SMS algorithms are $O\left(N_2 m_k^2 n_k + N_2 n_k^2 m_k\right)$, $O\left(N_1 m_k^2 n_k + N_1 n_k^2 m_k\right)$, $O\left(N_1^2 n_k^2 + N_1 n_k^3\right)$ and $O\left(n_k^{N_1}\right)$, respectively.

The average run time of each time step of the ET-LBP-ISMS, ET-LBP-SMS, ET-BP-SMS and JPDA-SMS algorithms are 0.143 s, 0.080 s, 0.258 s and 2.215 s, respectively, when $P_D = 0.99$. It can be seen that the ET-LBP-ISMS and ET-LBP-SMS algorithms are more efficient. The average run time of each time step of the ET-LBP-ISMS algorithm is longer than that of the ET-LBP-SMS algorithm. The reason for this is that more measurement cells in the ISMS increase the computational complexity in the LBP algorithm. It can also be seen that the ET-LBP algorithm significantly improves the efficiency of the ET-BP when the average time of ET-LBP-SMS and ET-BP-SMS algorithms are compared. The simulation results are consistent with the complexity analysis results mentioned above.

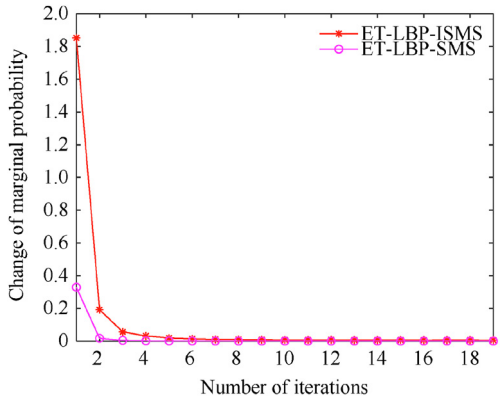

Fig. 6 Convergence of ET-LBP-ISMS and ET-LBP-ISMS algorithms.

In the LBP algorithm, an iteration terminates when the marginal posterior distribution does not change anymore or the number of iterations exceeds the maximum number of iterations. The change of marginal posterior distribution is evaluated by summing the difference between marginal posterior distributions in adjacent iterations. In order to analyze the scalability of the ET-LBP-ISMS and ET-LBP-SMS algorithms, Fig. 6 shows the average difference in marginal posterior distributions during iteration with $P_D = 0.99$. It can be seen that these two algorithms both have good convergence. They can almost reach convergence after the 8th iteration.

4.2.2. Scenario two

In case of $P_D = 0.99$, the TSRs of the ET-LBP-ISMS, ET-LBP-SMS, ET-BP-SMS and JPDA-SMS algorithms are 100%, 99.6%, 99.8% and 99.4%, respectively. It can be seen that the ET-LBP-ISMS algorithm is slightly better than the other algorithms in TSR. The position error and extension error of these algorithms are shown in Fig. 7 when $P_D = 0.99$. From Fig. 7(a), when targets are distant in space, it can be seen that these algorithms all perform well, and the ET-LBP algorithm has a smaller error in position estimation than the ET-BP algorithm. When targets are close in space, the ET-LBP-ISMS algorithm has a smaller error than the other algorithms in position estimation. Although the ET-LBP-SMS algorithm almost has the same performance with the JPDA-SMS algorithm in position estimation, it has more accurate extension state estimation, as shown in Fig. 7(b). Thus, compared with the ET-LBP-SMS, ET-BP-SMS and JPDA-SMS algorithms, the ET-LBP-ISMS algorithm is more robust when targets are close in space.

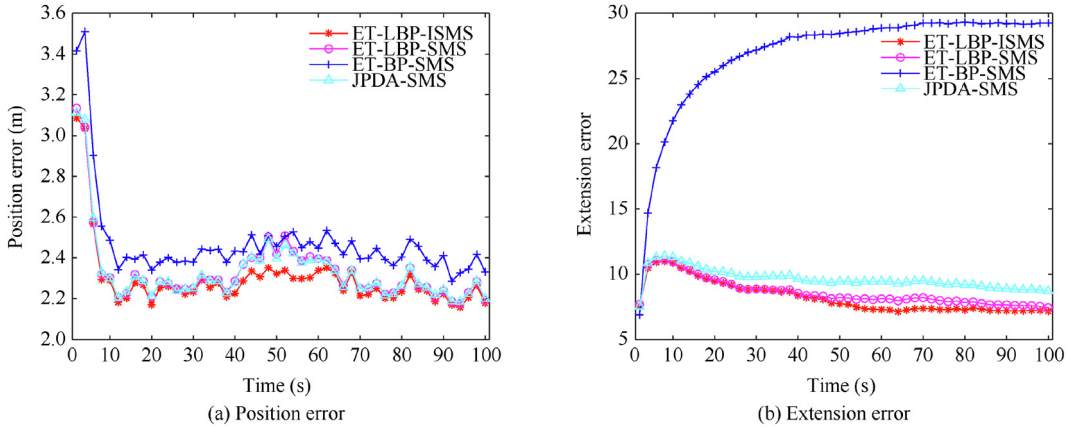

Fig. 7 Position error and extension error of ET-LBP-ISMS, ET-LBP-SMS, ET-BP-SMS and JPDA-SMS algorithms in scenario two when $P_D = 0.99$.

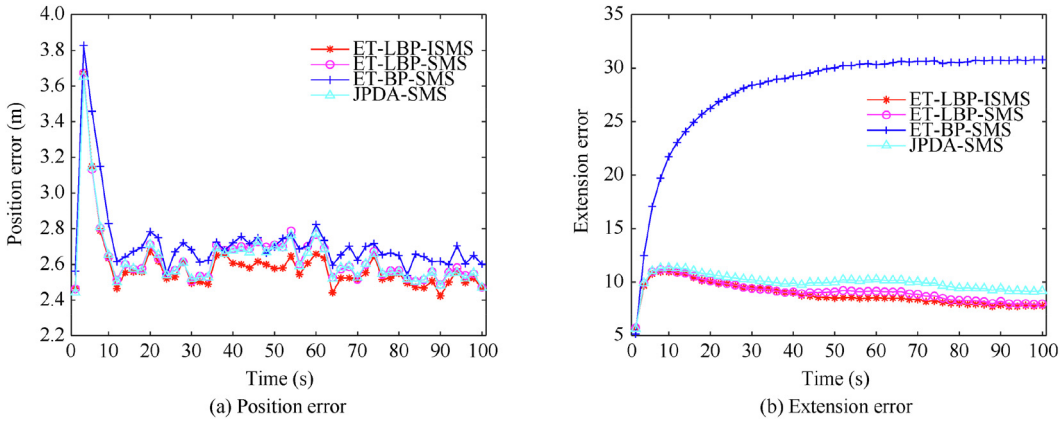

(a) Position error (b) Extension error

Fig. 8 Position error and extension error of ET-LBP-ISMS, ET-LBP-SMS, ET-BP-SMS and JPDA-SMS algorithms in scenario one when $P_D = 0.80$.

In case of $P_D = 0.80$, the TSRs of the ET-LBP-ISMS, ET-LBP-SMS, ET-BP-SMS and JPDA-SMS algorithms are 96.8%, 94.8%, 96.8% and 93.6%, respectively. The position error and extension error of these algorithms are shown in Fig. 8 when $P_D = 0.80$. Although all these algorithms have more significant errors in position and extension state estimation with lower P_D, they can all track targets well. The average run time of each time step of the ET-LBP-ISMS, ET-LBP-SMS, ET-BP-SMS and JPDA-SMS algorithms are 0.073 s, 0.050 s, 0.162 s and 0.075 s, respectively, when $P_D = 0.99$. It can also be seen that the ET-LBP-ISMS and ET-LBP-SMS algorithms are more efficient.

5. Conclusions

A new METT algorithm is proposed in this paper, named ET-LBP-ISMS. The algorithm is based on the graphical model with loops, which is solved by the LBP algorithm. At the same time, the ISMS is presented by adding some new measurement cells into the SMS. Based on Murty's algorithm[35] and the prediction information, these new measurement cells contain the K best associations for each target and the subpartition of big measurement cells. Simulations show that the ET-LBP algorithm has better accuracy than the ET-BP algorithm in terms of extension state estimation when they are implemented on the SMS. At the same time, the ET-LBP-ISMS algorithm has better performance in the kinematic state and extension state estimation. Therefore, the LBP algorithm can solve the data association problem of extended target tracking efficiently. Besides, although the RFS based algorithms avoid the data association problem, they still suffer from high computational complexity, especially in METT. Thus, researching more efficient METT algorithms based on RFS is also our future direction.

Acknowledgements

This work was supported by the National Natural Science Foundation of China (No. 61871301), National Natural Science Foundation of Shaanxi Province, China (No. 2018JQ6059) and Postdoctoral Science Foundation of China (No. 2018M633470).

References

1. Vo BN, Vo BT, Phung D. Labeled random finite sets and the Bayes multi-target tracking filter. *IEEE Trans Signal Process* 2014;**62**(24):6554–67.
2. Williams JL. Marginal multi-Bernoulli filters: RFS derivation of MHT, JIPDA, and association-based MeMBer. *IEEE Trans Aerosp Electron Syst* 2015;**51**(3):1664–87.
3. Beard M, Reuter S, Granström K, et al. Multiple extended target tracking with labeled random finite sets. *IEEE Trans Signal Process* 2015;**64**(7):1638–53.
4. Zhang YQ, Ji HB, Hu Q. A fast ellipse extended target PHD filter using box-particle implementation. *Mech Syst Signal Process* 2018;**99**:57–72.
5. Granström K, Orguner U. A PHD filter for tracking multiple extended targets using random matrices. *IEEE Trans Signal Process* 2012;**60**(11):5657–71.
6. Granström K, Lundquist C, Orguner O. Extended target tracking using a Gaussian-Mixture PHD filter. *IEEE Trans Aerosp Electron Syst* 2012;**48**(4):3268–86.
7. Bar-Shalom Y, Willett PK, Tian X. *Tracking and data fusion*. Storrs (CT): YBS; 2011.
8. Mahler R. *Statistical multisource multitarget information fusion*. Boston: Artech House; 2007.
9. Pearl J. *Probabilistic reasoning in intelligent systems*. San Francisco: Morgan Kaufmann; 1988.
10. Jordan MI. Graphical models. *Stat Sci* 2004;**19**(1):140–55.
11. Cowell RG, Dawid AP, Lauritzen SL, et.al. *Probabilistic networks and expert systems*. New York: Springer; 2007.
12. Meyer F, Kropfreiter T, Williams JL, et al. Message passing algorithms for scalable multitarget tracking. *Proc IEEE* 2018;**106**(2):221–59.
13. Ghazi RM, Chen JG, Büyüköztürk O. Pairwise graphical models for structural health monitoring with dense sensor arrays. *Mech Syst Signal Process* 2017;**93**:578–92.
14. Meyer F, Hlinka O, Wymeersch H, et al. Distributed localization and tracking of mobile networks including noncooperative objects. *IEEE Trans Signal Inf Process Networks* 2016;**2**(1):57–61.
15. Worthen AP, Stark WE. Unified design of iterative receivers using factor graphs. *IEEE Trans Inf Theory* 2001;**47**(2):843–9.
16. Berrou C, Glavieux A. Near optimum error correcting coding and decoding: Turbo-codes. *IEEE Trans Commun* 1996;**44**(10):1261–71.
17. Cetin M, Chen L, Fisher JW, et al. Distributed fusion in sensor networks. *IEEE Signal Process Mag* 2006;**23**(4):42–55.

18. Williams JL, Lau R. Approximate evaluation of marginal association probabilities with belief propagation. *IEEE Trans Aerosp Electron Syst* 2014;**50**(4):2942–59.
19. Meyer F, Braca P, Willett P, et al. A scalable algorithm of targets using multiple sensors. *IEEE Trans Signal Process* 2017;**65**(13):3478–93.
20. Su ZZ, Ji HB, Zhang YQ. Data association for extended target tracking by belief propagation. *IET Radar Sonar Navig* 2018;**12**(12):1484–92.
21. Kropfreiter T, Meyer F, Hlawatsch F. A fast labeled multi-bernoulli filter using belief propagation. *IEEE Trans Aerosp Electron Syst* 2019. Available from: https://doi.org/10.1109/TAES.2019.2941104.
22. Lundquist C, Granström K, Orguner U. An extended target CPHD filter and a Gamma Gaussian inverse Wishart implementation. *IEEE J Sel Top Signal Process* 2013;**7**(3):472–83.
23. Granström K, Orguner U. Estimation and maintenance of measurements rates for multiple extended target tracking. *IEEE international conference on information fusion*; 2012 Jul 9-12; Singapore. Piscataway: IEEE Press; 2012. p. 2170-6.
24. Granström K, Baum M, Reuter S. Extended object tracking: Introduction, overview and applications. *J Adv Inf Fusion* 2017;**12**(2):139–74.
25. Feldmann M, Fränken D, Koch JW. Tracking of extended objects and group targets using random matrices. *IEEE Trans Signal Process* 2011;**59**(4):1409–20.
26. Koch JW. Bayesian approach to extended object and cluster tracking using random matrices. *IEEE Trans Aerosp Electron Syst* 2008;**44**(33):1042–59.
27. Kschischang FR, Frey BJ, Loeliger HA. Factor graphs and the sum-product algorithm. *IEEE Trans Inf Theory* 2001;**47**(2):498–519.
28. Kidermann R, Snell JL. *Markov random fields and their applications*. Providence: AMS; 1980.
29. Jensen FV, Nielsen TD. *Bayesian networks and decision graphs*. New York: Springer-Verlag; 2007.
30. Riegler E, Kirkelund GE, Manchon CN, et al. Merging belief propagation and the mean field approximation: A free energy approach. *IEEE Trans Inf Theory* 2013;**59**(1):588–602.
31. Richardson TJ, Urbanke RL. The capacity of low-density parity-check codes under message-passing decoding. *IEEE Trans Inf Theory* 2001;**47**(2):599–618.
32. Ezlinger B, Meyer F, Hlawatsch F, et al. Cooperative simultaneous localization and synchronization in mobile agent networks. *IEEE Trans Signal Process* 2017;**65**(14):3587–602.
33. Chertkov M, Yedidia AB. Approximating the permanent with fractional belief propagation. *J Mach Learn Res* 2013;**14**:2029–66.
34. Bayati M, Shah D, Sharma M. Max-product for maximum weight matching: Convergence, correctness and LP duality. *IEEE Trans Inf Theory* 2008;**54**(3):1241–51.
35. Murty KG. An algorithm for ranking all the assignments in order of increasing cost. *Oper Res* 1968;**16**(3):682–7.

Please cite this article in press as: SU Z et al. Loopy belief propagation based data association for extended target tracking, *Chin J Aeronaut* (2020), https://doi.org/10.1016/j.cja.2020.01.004